

Non-Faradaic Electrochemical Promotion of Brønsted Acid-Catalyzed Dehydration Reactions over Molybdenum Oxide

Alexander A. Khechfe, Mark M. Sullivan, Dimitrios Zagoraios, Alexandros Katsaounis, Constantinos G. Vayenas, and Yuri Román-Leshkov*



Cite This: *ACS Catal.* 2022, 12, 906–912



Read Online

ACCESS |



Metrics & More



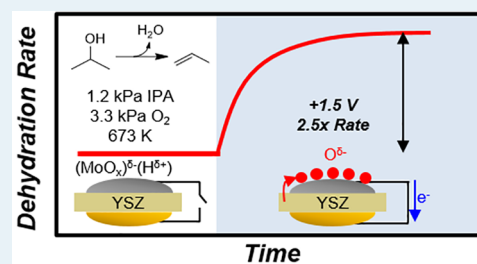
Article Recommendations



Supporting Information

ABSTRACT: We report the non-Faradaic electrochemical promotion of a Brønsted acid-catalyzed reaction over a metal oxide surface. Isopropanol dehydration to propylene was used as a probe reaction to study the *in situ* modification of a molybdenum catalyst film deposited on a yttria-stabilized zirconia solid electrolyte. Upon polarizing the Mo film by +1.5 V, the rate of isopropanol dehydration (1.2 kPa IPA, 3.3 kPa O₂, 673 K, 135 kPa total pressure) was enhanced by 2.5×. Smaller rate enhancements of c.a. 1.3× were also observed for 2-butanol dehydration to butenes over the same catalyst. Although electrochemical dehydration pathways for this chemistry are implausible, by postulating a hypothetical Faradaic dehydration route, we calculate Faradaic efficiencies greater than 100 for IPA dehydration, confirming the non-Faradaic nature of the promotional effect. This effect is reversible and does not appear to permanently alter the chemistry of the Mo film, based on XPS analysis. We hypothesize that this promotion originates from generation of Brønsted acid sites localized to the three-phase boundary at the catalyst/gas/electrolyte interface and/or acid site strengthening due to electrical polarization. This work demonstrates an alternative handle to promote catalytic turnover, which with further understanding, could be applied toward other Brønsted acid-catalyzed chemistries.

KEYWORDS: isopropanol dehydration, 2-butanol dehydration, MoO₃, Brønsted acid catalysis, electrochemical promotion/EPOC, NEMCA



INTRODUCTION

Temperature, pressure, and catalyst composition are typical handles to navigate the free energy landscape that controls reaction rates and product selectivities over heterogeneous catalyst surfaces. While tuning these three parameters has allowed for the design of countless catalytic systems over the last century, their limitations have driven researchers to look for more unconventional handles for tuning catalytic performance.^{1–3} In particular, electrochemical systems include the handle of the electrode potential, which can precisely modify the energy level of electrons on a catalyst electrode without modifying bulk process parameters. In these systems, the thermodynamics and kinetics of the reaction system can be directly related to the electrode potential via the Gibbs free energy and the Butler–Volmer equation, respectively.⁴ Vayenas and co-workers demonstrated that the electrode potential could also be used to modify thermocatalytic systems non-Faradaically, wherein reaction rates could reach significantly larger values than the simple addition of an electrochemical reaction rate to the thermocatalytic rate.⁵

In classic electrochemical promotion of catalysis (EPOC) systems, this phenomenon has been demonstrated by polarizing a thin metal film that is deposited on the surface of a solid ion-conductor pellet such as yttria-stabilized zirconia (YSZ). This metal film acts both as a catalyst and a working electrode

(WE) and is electrically connected to inert counter and reference electrodes (CE, RE) on the opposite side of the YSZ pellet. Upon anodic (i.e., positive) polarization of a WE catalyzing an oxidation reaction, gas-phase oxygen is reduced at the CE and pumped as O²⁻ ions through oxygen vacancies in the YSZ lattice. Upon reaching the WE, the O²⁻ moieties lose electrons to the circuit and form a double layer of adsorbed, partially charged O^{δ-} species with mirroring charges on the metal surface. Under typical reaction conditions ($T \sim 650$ K), applying ~ 1 V of polarization to the WE results in relatively small current flow (~ 1 – $1000 \mu\text{A}$); yet this polarization leads to drastic rate enhancements that far exceed the Faradaic current, resulting in Faradaic efficiencies above unity. For example, in ethylene oxidation over Pt films deposited on YSZ (643 K, $P_{\text{O}_2}/P_{\text{C}_2\text{H}_4} > 5$, $U_{\text{WR}} = 1$ V) rate enhancements up to a factor of 50 compared with the unpolarized state have been observed, corresponding to Faradaic efficiencies on the order

Received: October 25, 2021

Revised: December 6, 2021

of 10^3 – 10^4 (100 000%–1 000 000%).⁶ Additionally, polarization has also been shown to modify the selectivity of CO₂ hydrogenation to CO and CH₄ for noble metals deposited on various ion-conducting supports.^{7–9} In these studies, the dominant product was shifted from CO to CH₄ as the applied potential increased while holding temperature and reactant partial pressures constant. The EPOC effect is hypothesized to originate from the electrochemically forced reverse spillover of ionic species from the solid electrolyte (O^{δ-} in the case of YSZ) to the catalyst surface that can modify the local electronic environment at the catalyst surface.¹⁰ It has been shown using Kelvin probe techniques that in potential and temperature regimes allowing for reverse spillover, the change in the catalyst work function $\Delta\Phi_W$ directly correlates with the change in electrode potential of the working electrode, ΔU_{WR} , according to eq 1:^{5,10}

$$\Delta\Phi_W = e\Delta U_{WR} \quad (1)$$

The overwhelming majority of EPOC literature has focused on the promotion of redox reactions over noble metal catalysts.^{11–14} Only recently has there been increased interest in the use of EPOC for modifying reactions over non-noble transition metal and metal-oxide catalysts.^{15,16} To our knowledge, there have been no investigations on the effects of electrochemical modification to reactions catalyzed by solid Brønsted acids that exist on metal oxides such as MoO_x and WO_x, which are of critical importance in petrochemistry and for the upgrading of biomass-derived feedstocks.^{17,18}

Brønsted acid catalysis on metal oxides and carbides has been rigorously explored over the past few decades, and it has been shown that both the number of sites per gram of catalyst and the turnover rate over individual sites can be tuned via *in situ* and *ex situ* catalyst treatments. Brønsted acid sites on molybdenum and tungsten oxides can be formed via several means, including by reduction in hydrogen^{19–21} or protonation with alkanols.^{22,23} Baertsch et al. used ultraviolet visible diffuse reflectance spectroscopy to show that polytungstate domains supported on ZrO₂ were protonated by gaseous 2-butanol (2-BuOH) *in situ* during dehydration (0.5 kPa 2-BuOH, 323 K), resulting in the formation of reduced centers that are active for Brønsted acid catalysis.²² Additionally, IPA dehydration rates on MoO₃ catalysts (398 K, per g MoO₃) are dependent on the extent of MoO₃ partial reduction, leading to a nearly 100× increase in dehydration rates when reduced in pure H₂ for longer than 12 h at 623 K.²⁰ Rates of isopropanol (IPA) dehydration to propylene (415 K, 0.48 kPa IPA) over molybdenum carbide catalysts (Mo₂C) are also 10× higher in the presence of 13.5 kPa O₂ than under anaerobic conditions.²⁴ The turnover frequency (per Brønsted acid site) was found to hold a near-constant value of ~0.1 propylene s⁻¹ site⁻¹ despite large changes in rate at different oxygen partial pressures (0.03–3 μmol s⁻¹ g_{cat}⁻¹, 0–13 kPa O₂). The promotional effect was attributed to the formation of surface oxycarbides that can be subsequently protonated by gas-phase species to form Brønsted acid sites.

Given that the degree of oxidation/reduction of molybdena-based catalysts strongly influences subsequent activity for acid-catalyzed reactions, we hypothesized that the electrochemical supply of O^{δ-} species from a solid electrolyte should also influence reaction rates over solid acids. Here, we investigate the electrochemical promotion of redox-neutral, acid-catalyzed IPA dehydration using a Mo metal catalyst/WE supported on a YSZ pellet with Au CE and RE. IPA dehydration is an ideal

model reaction because it has only one major monomolecular acid-catalyzed dehydration product (propylene). While most studies of molybdena-based acid catalysts use MoO₃ as a starting material, we used Mo metal with a passivation oxide layer to allow electrical polarization across the WE. We show that acid-catalyzed IPA dehydration to propylene and diisopropyl ether (DIPE) can be reversibly promoted by applying anodic electrochemical potentials to the WE. This study expands the scope of EPOC as (i) a tunable handle to promote or modify acid catalysts *in situ* and (ii) to interface classical methods of heterogeneous catalysis research with electrochemistry to probe fundamental catalytic phenomena.

RESULTS AND DISCUSSION

DC magnetron sputtering of Mo onto the YSZ pellet resulted in a uniform film with a thickness of 330 nm (Figure S.2) and geometric surface area of 1.7 cm², corresponding to a total Mo mass of 0.6 mg. SEM images of the film are shown in Figures S.3a,b and reveal a structure that mirrors the morphology of the underlying YSZ surface. X-ray diffraction peaks were predominantly attributable to the YSZ solid electrolyte (Figure S.4); however, a small, broad peak was present centered near 41° that was attributed to crystalline Mo features.

For kinetic studies, the pellet was loaded into a CSTR reactor with a volume of 70 cm³ described in detail elsewhere^{5,11} and shown in Figure S.1. Briefly, the Mo/YSZ/Au pellet was held in place using a ceramic clamp which was suspended in the chamber via gold wires that also served as electrical connections to the three electrodes. A gold mesh (99.99% purity, Fisher Scientific) was placed between the gold wire and Mo film to ensure a continuous electrical contact over the entire working electrode. The reactor was placed in a furnace (Carbolite, GTF 11/50/150B) for temperature control. A K-type thermocouple monitored the temperature inside the reactor, which was controlled using a Cole-Parmer Digi-Sense Temperature Controller R/S 68900-11. Effluent gases were characterized using an Agilent 8890 gas chromatograph equipped with a flame ionization detector (FID) and a 30 m Agilent Poraplot-Q column.

Introduction of 1.2 kPa IPA and 3.3 kPa O₂ at 673 K into the CSTR resulted in monomolecular dehydration of IPA to propylene, bimolecular dehydration to form DIPE, and dehydrogenation to form acetone. A typical open circuit potential (OCP) value under these conditions was 0.13 V vs the Au reference electrode. The OCP appeared to vary in a Nernstian fashion consistent with a two-electron transfer between IPA and acetone (Figure S.5). The dehydration and dehydrogenation rates changed negligibly with total flow rate, allowing the system to be approximated as a CSTR with no external mass transfer limitations (Figure S.6). In the absence of an O₂ cofeed, propylene formation rates fell to <5% of the value in the presence of O₂ (Figure S.7), indicating that an overly reduced surface does not sustain the acidic species necessary to catalyze dehydration reactions. At temperatures above 673 K, the conductivity of YSZ is high enough to yield a current flow (>1 μA) sufficiently large to carry out EPOC studies. However, this temperature is too high to guarantee irreversible binding of a titrant (such as 2,6-di-*tert*-butylpyridine, DTBP) that could confirm the presence of Brønsted acid sites. To infer the presence of Brønsted acid sites, a separate fixed bed reactor with a metallic Mo catalyst was exposed to identical reactant concentrations at 423 K. Introduction of DTBP reversibly shut off activity to both

propylene and DIPE (Figure S.8). DTBP is known to exclusively poison Brønsted acid sites, as it is sterically hindered from poisoning Lewis acid sites.²² These data implicated that catalytic activity on our Mo film is due to Brønsted acid sites.

Immediate deactivation in the propylene and acetone formation rates was observed upon introduction of the reactant feeds (Figures S.8 and S.9). Propylene reaction rates decayed by ~15% over ~24 h with slight differences in deactivation rates based on sample preparation. The rate of acetone formation decayed to the homogeneous oxidative dehydrogenation (ODH) rate after approximately 70 h on stream, indicating a loss of metallic sites capable of catalyzing ODH over time. The rate of DIPE formation was ~3 orders of magnitude lower than the rate of propylene formation and initially increased with time on stream, but began to decay after ~120 h on stream. Propylene formation rates were corrected using a first-order deactivation model and are reported as such unless otherwise noted (see SI section S.3, Figures S.9–S.12). Deactivation mechanisms are still the subject of study, but a loss of geometric surface area after extended times on stream (Figure S.12) indicates that MoO_x sintering or sublimation may be contributing factors.^{25–27}

Application of +1.5 V (vs the Au reference) to the Mo electrode at constant reaction conditions (1.2 kPa IPA, 3.3 kPa O₂, 673 K) resulted in an increase in the monomolecular and bimolecular dehydration rates by factors of 2.5 and 1.4, respectively, over the course of a 6-h transient (Figure 1). In

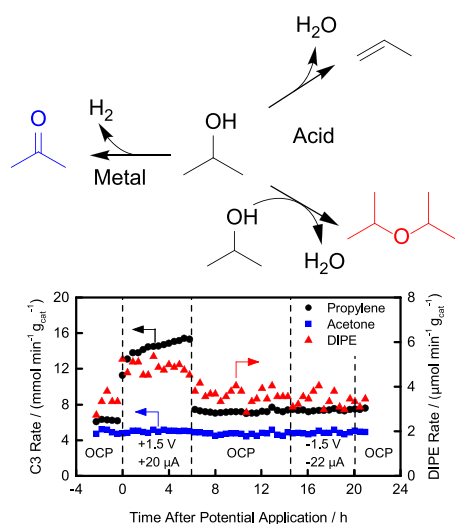


Figure 1. Rate of propylene, acetone, and DIPE formation (per g) over the Mo film in the CSTR-like reactor under open circuit, +1.5 V, and -1.5 V application. Reaction conditions: 673 K, 1.2 kPa IPA, 3.3 kPa O₂, total pressure 135 kPa (balance He/N₂), total flow rate 232 mL min⁻¹. Propylene rates are deactivation corrected.

contrast, the acetone formation rate did not vary with applied potential, indicating that anodic electrical polarization has no impact on dehydrogenation chemistry under these conditions. Return to OCP conditions resulted in both dehydration rates decaying back to within 20% of their open circuit values prior to potential application, indicating that anodic polarization does not permanently modify the chemical or physical structure of the catalyst surface. Figure S.13 shows the reversibility and repeatability of promotion upon anodic

polarization at long times on stream (>60 h). Even after several anodic potential excursions, the promotion effect is reversible and does not permanently affect the catalyst surface.

Cathodic polarization to -1.5 V resulted in no observable change to reaction rates or selectivities, indicating that this promotional effect is unique to anodic polarization. This asymmetry in the promotion about the OCP rules out the possibility of Joule heating as the cause of the observed increased rates under polarization. Given that the magnitude of current driven upon cathodic and anodic polarization is similar, the heating rate of the catalyst (proportional to I^2R , where R is the resistance of the film) should also be the same. If Joule heating were the cause of this rate promotion, local exotherms and subsequent promotional effects upon the reaction rate should be comparable for both directions of polarization.

Although the additive effects of a thermocatalytic and electrocatalytic rate could be postulated as the reason for the potential-induced rate enhancement, we note that dehydration reactions are redox neutral and thus cannot electrochemically occur at a single electrode. In this solid–gas phase system, YSZ is only responsible for mediating the transport of O²⁻ ions and does not contribute to measured reaction rates (Figure S.11).^{28,29} While numerous hypothetical dehydration reaction schemes could be facilitated by gas-phase ions or radical species, these species would need to be long-lived enough to ferry charge between the working and counter electrodes by traversing the gas-phase, which should not be a primary driver of the rate enhancement at the reaction conditions. Although electrochemical dehydration pathways are implausible, we calculated a pseudo-Faradaic efficiency, Λ , to further prove that the observed rate enhancement cannot be the result of an additional electrochemical reaction. This pseudo-Faradaic efficiency can be calculated from the rate data in Figure 1 and by assuming a 1:1 stoichiometry of supplied O²⁻ ions to formed propylene, as shown in eq 2.

$$\text{Faradaic efficiency} = \Lambda = \frac{\Delta r}{I/2F} \left(\frac{\text{mol O}^{2-}}{\text{mol C}_3\text{H}_6} \right) = 958 \quad (2)$$

where F is Faraday's constant and I is the total supplied current. This Faradaic efficiency calculates the increase in observed dehydration rate (Δr) to the rate of supplied O²⁻ ions ($I/2F$) and is an absolute lower bound on a hypothetical Faradaic efficiency because of the assumption of a 1:1 stoichiometry of supplied O²⁻ ions to formed propylene. The calculated Faradaic efficiency of 958 (95 800%) demonstrates that every O²⁻ spilling over from the YSZ results in 958 extra dehydration turnovers, clearly demonstrating that the promotional effect observed upon anodic polarization is indeed due to a non-Faradaic modification to the Mo catalytic surface. When using propylene rates without correcting for deactivation to calculate a pseudo-Faradaic efficiency, Λ decreases to 161 (16 100%), indicating non-Faradaic behavior regardless of how one chooses to calculate the Faradaic efficiency in this system.

To gain quantitative insight into the nature of the non-Faradaic promotion, we measured potential dependence, apparent activation energies, and reaction orders by measuring the monomolecular dehydration rate as a function of applied potential (0–1.5 V vs Au), temperature (653–693 K, OCP and +1.5 V), and IPA partial pressure (0.31–4.83 kPa, OCP and +1.5 V). Figure 2a shows the propylene formation rate dependence on applied anodic potential. Relatively modest

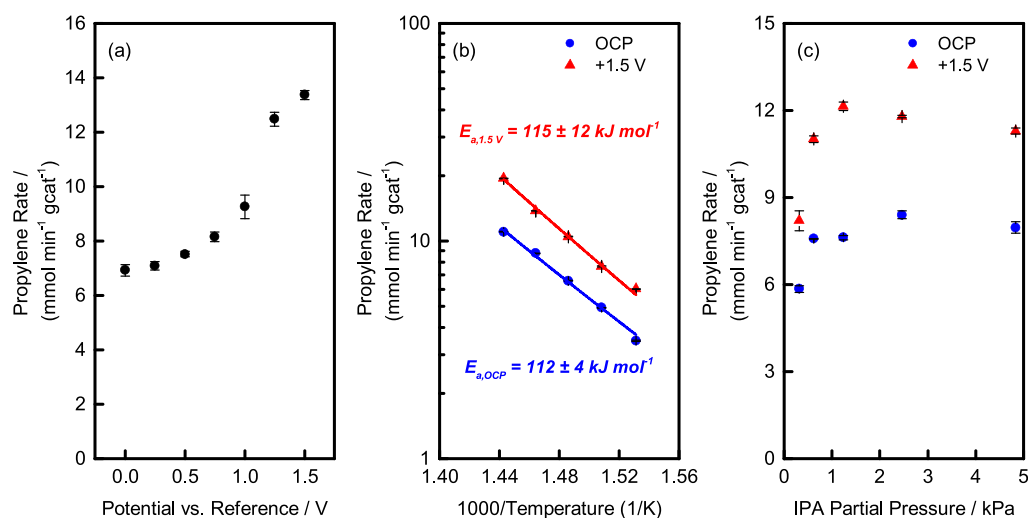


Figure 2. (a) Dependence of dehydration rate upon the applied potential between the Mo working electrode and Au reference electrode (673 K, 1.2 kPa of IPA, 3.3 kPa of O₂, 135 kPa total pressure, 232 mL min⁻¹ total flow) (b) Dehydration rate measured as a function of inverse temperature (1.2 kPa IPA, 3.3 kPa O₂, 135 kPa total pressure, 232 mL min⁻¹ total flow, balance He/N₂) at open circuit and while applying +1.5 V to the Mo working electrode. (c) Dehydration rate as a function of P_{IPA} (673 K, 3.3 kPa O₂, 135 kPa total pressure) at open circuit and while applying +1.5 V to the Mo working electrode.

rate enhancements are observed until a steeper change above 1.0 V vs Au, followed by another small increase between 1.25 and 1.5 V. This behavior is qualitatively similar to other EPOC systems, wherein substantial rate enhancements are only observed after considerable overpotentials are applied to the WE.^{6,30} This rate behavior is commonly attributed to an increase in surface coverages of promotional O^{δ-} species at higher applied potentials or currents.

Figure 2b shows the monomolecular dehydration rate as a function of temperature at open circuit and at +1.5 V. The activation energy under anodic polarization is statistically indistinguishable from the OCP activation energy. Given a roughly 2-fold rate enhancement at +1.5 V, the maximum activation energy difference that could be expected would only be about 4 kJ/mol, assuming the Arrhenius prefactor is unchanged. Thus, activation energies at open and closed circuit conditions should be experimentally indistinguishable.

Figure 2c shows that the rate of IPA dehydration at OCP initially increased with IPA partial pressure before reaching a zero-order regime at <1 kPa IPA, indicating that the surface is rapidly saturated with the reactant IPA in a typical Langmuirian fashion, in agreement with dehydration mechanisms that proceed through either E₁ or E₂ routes as is discussed in Section S.4. This also implicates that the calculated activation energy is the intrinsic activation energy that compares the energies of the bound surface intermediate and an expected carbocation transition state. Under closed circuit conditions, varying the IPA partial pressure reveals three kinetic regimes. For partial pressures below 1.2 kPa, the IPA dehydration rate is positive order in IPA partial pressure. The rate order then passes through a zero-order regime before transitioning to a slight negative order dependence at higher IPA pressures. In alcohol dehydration systems, reactant inhibition typically implies the formation of alcohol dimers on the surface, which inhibit monomolecular dehydration pathways.^{31–33}

Electrochemical promotion was also observed for 2-BuOH dehydration to butenes on a pellet previously used for IPA

dehydration. Introduction of 0.4 kPa 2-BuOH and 3.2 kPa O₂ (227 mL min⁻¹ total flow rate) at 673 K led to the formation of 1-butene, *trans*-2-butene, and *cis*-2-butene with selectivities of 19%, 27%, and 54%, respectively. Isobutene, which typically forms via skeletal isomerization of other butene products,³⁴ was not observed. Figure 3 shows that polarizing to +1.5 V led

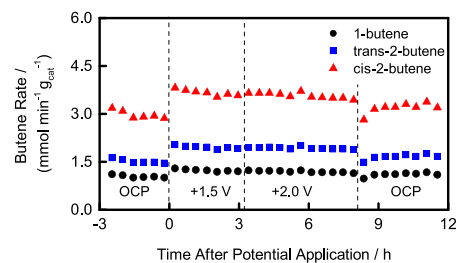


Figure 3. 2-BuOH dehydration rate to butene isomers over a Mo film previously used for IPA dehydration at open circuit, +1.5 V, and +2 V. Reaction conditions: 673 K, 0.4 kPa 2-BuOH, 3.2 kPa O₂, total pressure 128 kPa (balance He/N₂), total flow rate 227 mL min⁻¹. 2-BuOH dehydration rates were stable over the course of the experiment and did not require deactivation correction.

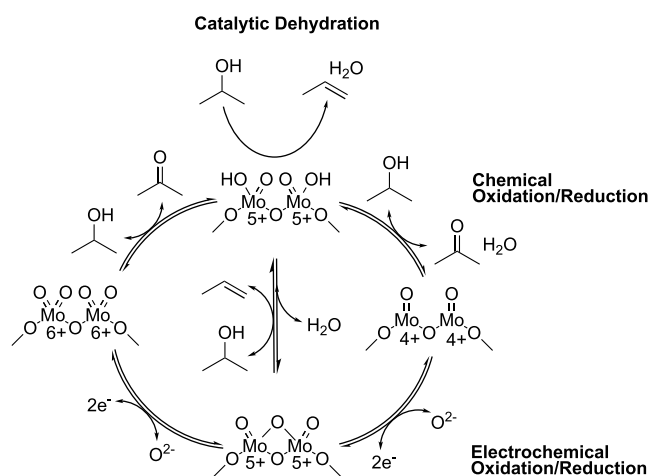
to rate enhancements for 1-butene, *trans*-2-butene, and *cis*-2-butene of 1.3×, 1.4×, and 1.3×, respectively, indicating that anodic polarization affects all 2-BuOH dehydration pathways to approximately the same extent. Increasing the voltage to +2.0 V led to no further rate enhancement. At 673 K, the equilibrium composition of these three butene isomers is expected to be 21.5% 1-butene, 42.8% *trans*-2-butene, and 35.8% *cis*-2-butene (see SI Section S.4 for calculations), indicating that the system is (1) not equilibrated at open circuit and (2) anodic polarization does not appreciably shift the product distribution toward or away from equilibrium. Taken together, these data show that the electrochemical promotion of Brønsted acid catalysis is general for alkanol

dehydration and has the potential to be applied to more complex substrates.

We have demonstrated that Brønsted acid-catalyzed isopropanol and 2-butanol monomolecular dehydration rates can be promoted by factors of 2.5× and 1.3×, respectively, via application of an external electrochemical potential. This promotional effect is non-Faradaic in nature and exclusively occurs during anodic polarization. In metallic EPOC systems, rate enhancement upon electrochemical polarization is ascribed to a concomitant change in the metal's work function. For a Brønsted acid catalyst, rate enhancement must arise from a different phenomenon. While elucidating the exact mechanism for this promotion is the subject of future work, we postulate two possible routes through which this promotion occurs.

The first possible explanation for this promotion is that anodic polarization of the Mo film changes the average oxidation state of the MoO_x surface, thus generating more Brønsted acid sites. A molybdenum moiety of intermediate oxidation state, hypothesized to be Mo(V) ,^{20,35–37} catalyzes isopropanol dehydration via either a Lewis acidic functionality or Brønsted acidic hydroxyl groups. In the absence of any potential-driven current, the oxidation states of surface MoO_x moieties are mediated by the gaseous atmosphere, where isopropanol can serve as a gas-phase reductant and O_2 or acetone can serve as gaseous oxidants. While electrochemical oxidation of the catalyst is not typically considered for noble metals such as Pt or Pd, electrode oxidation has been detected during electrochemical promotion of FeO_x ¹⁵ and CoO_x ¹⁶ films for the reverse water gas shift reaction. In these systems, the oxidation state of the film is a function of the electrochemical potential, temperature, and atmosphere. Scheme 1 depicts a

Scheme 1. Proposed Mechanism for *In Situ* Modification of Acid Site Densities of a Mo Film by Electrochemical Oxidation via Oxygen Anions (Bottom Pathways) and Chemical Reduction via Isopropanol Protonation (Top Pathways)



hypothesized mechanism of generation of new Brønsted acid sites over the MoO_x surface mediated by electrochemical oxidation from potential application and chemical reduction from atmospheric IPA.

To probe changes to the surface Mo oxidation state based on potential application, XPS spectra were taken of a pristine Mo film before being loaded into the reactor (Figure 4a), after

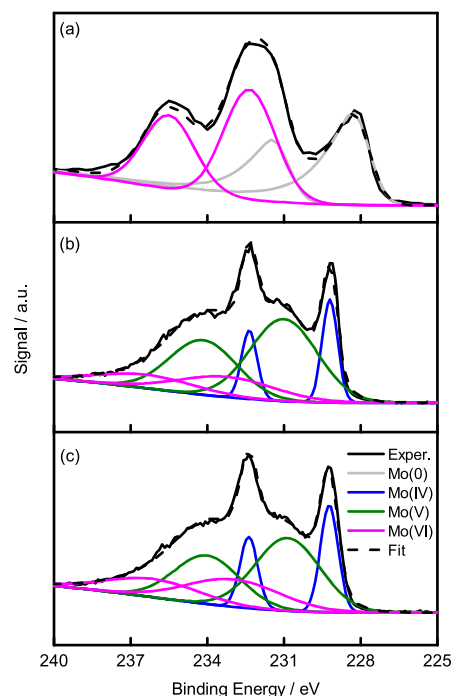


Figure 4. XPS spectra of the Mo 3d peaks taken on a pellet (a) prior to loading into the reactor, (b) after 15 h at 673 K with 1.2 kPa IPA and 3.3 kPa O_2 , and (c) after having been polarized at +1.5 V under the conditions in (b) for 3 h.

exposure to reaction conditions for 15 h (Figure 4b), and after being polarized at +1.5 V for 3 h followed by immediate purging in He gas and cooling to room temperature (Figure 4c). Only metallic Mo and a passivated Mo(VI) layer were observed on the pristine film, while a mixture of Mo(IV) , Mo(V) , and Mo(VI) were observed after reaction and polarization. A large-scale change to the Mo oxidation state at the surface of the catalyst upon polarization would manifest itself as an appreciable increase in the amount of Mo(V) obtained after Mo 3d peak deconvolution, assuming this change were long-lived enough to persist between potential shut-off, cooling, and spectra acquirement (~ 3 h).

Table 1 shows the relative composition of Mo oxidation states based on the XPS spectra in Figure 4. Given the nominal

Table 1. Relative Surface Compositions (mol %) of Different Mo Oxidation States on a Mo Pellet before Reaction, after 15 h on Stream, and after 3 h of Polarization, as Obtained by XPS

film	Mo(0)	Mo(IV)	Mo(V)	Mo(VI)
pristine	34.7	0	0	65.3
15 h on stream	0	17.7	60.8	21.5
postpolarization	0	20.7	51.5	27.8

difference in chemical makeup of the Mo peaks between Figure 4b (pre-polarization) and Figure 4c (post-polarization), it can be inferred that large-scale, long-lived oxidation of the Mo surface is unlikely to take place upon electrochemical polarization. A lack of features in cyclic voltammograms taken under the

reaction conditions (Figure S.14) further undermines the possibility of large-scale electrochemical Mo oxidation. Thus, if electrochemical polarization results in the generation of catalytically active Mo(V) sites from Mo(IV) or Mo(0), it is likely to be at a small scale localized to the three-phase boundary where O* species spill over from the YSZ onto the electrode surface.

The second possible origin for this promotional effect is that polarization changes the relative stability of surface intermediates and/or transition states. When a proton is removed from a catalyst surface, the resulting metal oxide accumulates a negative charge to counterbalance the proton.^{38,39} Increased deprotonation energies, corresponding to increased activation barriers for 2-BuOH dehydration and decreased stability of 2-BuOH dimers, were observed on W and Mo-based polyoxometalates (POM) with compositions or coadsorbates that transfer electron density into the metal oxide shell of the POM.⁴⁰ By contrast, an adsorbate that removes electron density from the oxide surface, such as O^{δ-}, might be expected to decrease deprotonation energies and thus strengthen Brønsted acid sites. If reverse spillover O^{δ-} species modify the semiconducting MoO_x film by decreasing the electrochemical potential of electrons in the film as they do on metals, the film may better accept charge from the conjugate base after deprotonation, resulting in stronger Brønsted acid sites and increased dehydration rates.

CONCLUSIONS

In conclusion, we have demonstrated the first reported instance of a non-Faradaic electrochemical promotion of a gas-phase solid acid-catalyzed reaction. The results demonstrate the feasibility of combining the fine control of applied electrochemical potential in a typical thermocatalytic reaction system to reversibly and controllably modify the function of a catalytic material to affect redox-neutral Brønsted acid catalysis. This concept can be explored extensively by thorough kinetic studies, spectroscopy, and density functional theory calculations. This idea can also be extended to other acid-catalyzed chemistries with different electrodes and ion conductors. This work represents a critical bridge between of the fields of electrochemistry and thermal catalysis and offers new opportunities to promote catalytic events with unconventional handles.

ASSOCIATED CONTENT

Supporting Information

The Supporting Information is available free of charge at <https://pubs.acs.org/doi/10.1021/acscatal.1c04885>.

S.1 Detailed Experimental Procedures; S.2 Catalyst Characterization (SEM, XRD, OCP data); S.3 Supplemental Reactivity Studies (space velocity tests, O₂ dependence, Brønsted acid titration, deactivation correction, replicates); S.4 Derivation of Monomolecular Dehydration Rate Law; S.5 Butene Isomer Equilibrium Calculations (PDF)

AUTHOR INFORMATION

Corresponding Author

Yuriy Román-Leshkov – Department of Chemical Engineering, Massachusetts Institute of Technology, Cambridge, Massachusetts 02139, United States;

orcid.org/0000-0002-0025-4233; Email: yroman@mit.edu

Authors

Alexander A. Khechfe – Department of Chemical Engineering, Massachusetts Institute of Technology, Cambridge, Massachusetts 02139, United States

Mark M. Sullivan – Department of Chemical Engineering, Massachusetts Institute of Technology, Cambridge, Massachusetts 02139, United States; orcid.org/0000-0002-1765-4129

Dimitrios Zagoraios – Department of Chemical Engineering, University of Patras, 26504 Patras, Greece

Alexandros Katsaounis – Department of Chemical Engineering, University of Patras, 26504 Patras, Greece; orcid.org/0000-0001-6634-6459

Constantinos G. Vayenas – Department of Chemical Engineering, University of Patras, 26504 Patras, Greece; Academy of Athens, 10679 Athens, Greece

Complete contact information is available at: <https://pubs.acs.org/10.1021/acscatal.1c04885>

Notes

The authors declare no competing financial interest.

ACKNOWLEDGMENTS

We thank John R. Di Iorio (J.R.D.) and Thejas S. Wesley for helpful technical advice and scientific discussions. We further thank J.R.D. for valuable feedback on the manuscript. Studies were supported by a Prof. Amar G. Bose Research Program Grant from MIT. Additional support was provided by the U.S. Department of Energy, Office of Basic Energy Sciences under Award DE-SC0016214. This work made use of the MRSEC Shared Experimental Facilities at MIT, supported by the National Science Foundation under award number DMR-1419807. A.A.K. acknowledges support from the National Science Foundation Graduate Research Fellowship under Grant No. 1745302. Any opinion, findings, and conclusions or recommendations expressed in this material are those of the authors(s) and do not necessarily reflect the views of the National Science Foundation.

REFERENCES

- Hülsey, M. J.; Lim, C. W.; Yan, N. Promoting Heterogeneous Catalysis beyond Catalyst Design. *Chem. Sci.* **2020**, *11* (6), 1456–1468.
- Shetty, M.; Walton, A.; Gathmann, S. R.; Ardagh, M. A.; Gopeesingh, J.; Resasco, J.; Birol, T.; Zhang, Q.; Tsapatsis, M.; Vlachos, D. G.; et al. The Catalytic Mechanics of Dynamic Surfaces: Stimulating Methods for Promoting Catalytic Resonance. *ACS Catal.* **2020**, *10* (21), 12666–12695.
- Che, F. L.; Gray, J. T.; Ha, S.; Kruse, N.; Scott, S. L.; McEwen, J. S. Elucidating the Roles of Electric Fields in Catalysis: A Perspective. *ACS Catal.* **2018**, *8* (6), 5153–5174.
- Gileadi, E. *Physical Electrochemistry: Fundamentals, Techniques and Applications*; Wiley-VCH: Weinheim, 2011.
- Vayenas, C. G.; Bebelis, S.; Pliangos, C.; Brosda, S.; Tsipalides, D. *Electrochemical Activation of Catalysis: Promotion, Electrochemical Promotion, and Metal-Support Interactions*; Springer Science & Business Media, 2001.
- Bebelis, S.; Vayenas, C. G. Non-Faradaic Electrochemical Modification of Catalytic Activity. I. The Case of Ethylene Oxidation on Pt. *J. Catal.* **1989**, *118* (1), 125–146.
- Kotsiras, A.; Kalaitzidou, I.; Grigoriou, D.; Symillidis, A.; Makri, M.; Katsaounis, A.; Vayenas, C. G. Electrochemical Promotion of

- Nanodispersed Ru-Co Catalysts for the Hydrogenation of CO₂. *Appl. Catal., B* **2018**, *232*, 60–68.
- (8) Zagoraios, D.; Panaritis, C.; Krassakopoulou, A.; Baranova, E. A.; Katsaounis, A.; Vayenas, C. G. Electrochemical Promotion of Ru Nanoparticles Deposited on a Proton Conductor Electrolyte during CO₂ Hydrogenation. *Appl. Catal., B* **2020**, *276*, 119148.
- (9) Panaritis, C.; Zgheib, J.; Couillard, M.; Baranova, E. A. The Role of Ru Clusters in Fe Carbide Suppression for the Reverse Water Gas Shift Reaction over Electropromoted Ru/FeOx Catalysts. *Electrochem. Commun.* **2020**, *119*, 106824.
- (10) Vayenas, C. G.; Bebelis, S.; Ladas, S. Dependence of Catalytic Rates on Catalyst Work Function. *Nature* **1990**, *343* (6259), 625–627.
- (11) Zagoraios, D.; Athanasiadi, A.; Kalaitzidou, I.; Ntais, S.; Katsaounis, A.; Caravaca, A.; Vernoux, P.; Vayenas, C. G. Electrochemical Promotion of Methane Oxidation over Nanodispersed Pd/Co₃O₄ Catalysts. *Catal. Today* **2020**, *355*, 910–920.
- (12) Kalaitzidou, I.; Makri, M.; Theleritis, D.; Katsaounis, A.; Vayenas, C. G. Comparative Study of the Electrochemical Promotion of CO₂ Hydrogenation on Ru Using Na⁺, K⁺, H⁺ and O₂ – Conducting Solid Electrolytes. *Surf. Sci.* **2016**, *646*, 194–203.
- (13) Vernoux, P. Recent Advances in Electrochemical Promotion of Catalysis. *Catalysis* **2017**, *29*, 29–59.
- (14) Jahromi, A. F.; Ruiz-López, E.; Dorado, F.; Baranova, E. A.; de Lucas-Consuegra, A. Electrochemical Promotion of Ethanol Partial Oxidation and Reforming Reactions for Hydrogen Production. *Renewable Energy* **2022**, *183*, 515–523.
- (15) Panaritis, C.; Zgheib, J.; Ebrahim, S. A. H.; Couillard, M.; Baranova, E. A. Electrochemical In-Situ Activation of Fe-Oxide Nanowires for the Reverse Water Gas Shift Reaction. *Appl. Catal., B* **2020**, *269*, 118826.
- (16) Zagoraios, D.; Tsatsos, S.; Kennou, S.; Vayenas, C. G.; Kyriakou, G.; Katsaounis, A. Tuning the RWGS Reaction via EPOC and In Situ Electro-Oxidation of Cobalt Nanoparticles. *ACS Catal.* **2020**, *10*, 14916–14927.
- (17) Settle, A. E.; Berstis, L.; Rorrer, N. A.; Roman-Leshkóv, Y.; Beckham, G. T.; Richards, R. M.; Vardon, D. R. Heterogeneous Diels-Alder Catalysis for Biomass-Derived Aromatic Compounds. *Green Chemistry* **2017**, *19*, 3468–3492.
- (18) Shetty, M.; Anderson, E. M.; Green, W. H.; Román-Leshkov, Y. Kinetic Analysis and Reaction Mechanism for Anisole Conversion over Zirconia-Supported Molybdenum Oxide. *J. Catalysis* **2019**, *376*, 248.
- (19) Uchijima, F.; Takagi, T.; Itoh, H.; Matsuda, T.; Takahashi, N. Catalytic Properties of H₂-Reduced MoO₃ with Noble Metal for the Conversions of Heptane and Propan-2-ol. *Phys. Chem. Chem. Phys.* **2000**, *2* (5), 1077–1083.
- (20) Matsuda, T.; Hirata, Y.; Sakagami, H.; Takahashi, N. Catalytic Properties of MoO₃ Reduced at Different Temperatures for the Conversions of Heptane and 2-Propanol. *Microporous Mesoporous Mater.* **2001**, *42* (2–3), 345–353.
- (21) Macht, J.; Iglesia, E. Structure and Function of Oxide Nanostructures: Catalytic Consequences of Size and Composition. *Phys. Chem. Chem. Phys.* **2008**, *10* (35), 5331–5343.
- (22) Baertsch, C. D.; Komala, K. T.; Chua, Y. H.; Iglesia, E. Genesis of Brønsted Acid Sites during Dehydration of 2-Butanol on Tungsten Oxide Catalysts. *J. Catal.* **2002**, *205* (1), 44–57.
- (23) Macht, J.; Baertsch, C. D.; May-Lozano, M.; Soled, S. L.; Wang, Y.; Iglesia, E. Support Effects on Brønsted Acid Site Densities and Alcohol Dehydration Turnover Rates on Tungsten Oxide Domains. *J. Catal.* **2004**, *227* (2), 479–491.
- (24) Sullivan, M. M.; Held, J. T.; Bhan, A. Structure and Site Evolution of Molybdenum Carbide Catalysts upon Exposure to Oxygen. *J. Catal.* **2015**, *326*, 82–91.
- (25) Zhang, W.; Desikan, A.; Oyama, S. T. Effect of Support in Ethanol Oxidation on Molybdenum Oxide. *J. Phys. Chem.* **1995**, *99* (39), 14468–14476.
- (26) Bedard, J.; Hong, D. Y.; Bhan, A. CH₄ Dehydroaromatization on Mo/H-ZSM-5: I. Effects of Co-Processing H₂ and CH₃COOH. *J. Catal.* **2013**, *306*, 58–67.
- (27) Guimond, S.; Gobke, D.; Sturm, J. M.; Romanyshyn, Y.; Kuhlbeck, H.; Cavalleri, M.; Freund, H.-J. Well-Ordered Molybdenum Oxide Layers on Au(111): Preparation and Properties. *J. Phys. Chem. C* **2013**, *117*, 8746.
- (28) Hui, S.; Roller, J.; Yick, S.; Zhang, X.; Decès-Petit, C.; Xie, Y.; Maric, R.; Ghosh, D. A Brief Review of the Ionic Conductivity Enhancement for Selected Oxide Electrolytes. *J. Power Sources* **2007**, *172*, 493–502.
- (29) Ahamer, C.; Opitz, A. K.; Rupp, G. M.; Fleig, J. Revisiting the Temperature Dependent Ionic Conductivity of Yttria Stabilized Zirconia (YSZ). *J. Electrochem. Soc.* **2017**, *164* (7), F790–F803.
- (30) Marina, O. A.; Yentekakis, I. V.; Vayenas, C. G.; Palermo, A.; Lambert, R. M. In Situ Controlled Promotion of Catalyst Surfaces via NEMCA: The Effect of Na on the Pt-Catalyzed NO Reduction by H₂. *J. Catal.* **1997**, *166* (2), 218–228.
- (31) Zhi, Y.; Shi, H.; Mu, L.; Liu, Y.; Mei, D.; Camaioni, D. M.; Lercher, J. A. Dehydration Pathways of 1-Propanol on HZSM-5 in the Presence and Absence of Water. *J. Am. Chem. Soc.* **2015**, *137* (50), 15781–15794.
- (32) Macht, J.; Janik, M. J.; Neurock, M.; Iglesia, E. Mechanistic Consequences of Composition in Acid Catalysis by Polyoxometalate Keggin Clusters. *J. Am. Chem. Soc.* **2008**, *130* (31), 10369–10379.
- (33) Kang, M.; DeWilde, J. F.; Bhan, A. Kinetics and Mechanism of Alcohol Dehydration on γ -Al₂O₃: Effects of Carbon Chain Length and Substitution. *ACS Catal.* **2015**, *5* (2), 602–612.
- (34) Houzvička, J.; Ponec, V. Skeletal Isomerization of *n*-Butene. *Catal. Rev.: Sci. Eng.* **1997**, *39* (4), 319–344.
- (35) Matsuda, T.; Sakagami, H.; Takahashi, N. Thermal Stability of Porous MoOx and Its Catalytic Property for the Conversion of 2-Propanol. *Appl. Catal., A* **2001**, *213* (1), 83–90.
- (36) Matsuda, T.; Ohno, T.; Sakagami, H.; Takahashi, N. Reduction of MoO₃ to Porous Molybdenum Oxides and Its Catalytic Properties for Alkane Isomerization. *J. Jpn. Pet. Inst.* **2007**, *50* (5), 229–239.
- (37) Suarez, W.; Dumesic, J. A.; Hill, C. G. Acidic Properties of Molybdena-Alumina for Different Extents of Reduction: Infrared and Gravimetric Studies of Adsorbed Pyridine. *J. Catal.* **1985**, *94* (2), 408–421.
- (38) Deshlahra, P.; Carr, R. T.; Iglesia, E. Ionic and Covalent Stabilization of Intermediates and Transition States in Catalysis by Solid Acids. *J. Am. Chem. Soc.* **2014**, *136* (43), 15229–15247.
- (39) Deshlahra, P.; Iglesia, E. Toward More Complete Descriptors of Reactivity in Catalysis by Solid Acids. *ACS Catal.* **2016**, *6* (8), 5386–5392.
- (40) Janik, M. J.; Macht, J.; Iglesia, E.; Neurock, M. Correlating Acid Properties and Catalytic Function: A First-Principles Analysis of Alcohol Dehydration Pathways on Polyoxometalates. *J. Phys. Chem. C* **2009**, *113* (5), 1872–1885.